

---

# UAV3D: A Large-scale 3D Perception Benchmark for Unmanned Aerial Vehicles

---

**Hui Ye**  
Dept. of Computer Science  
Georgia State University  
Atlanta, GA 30303  
hye2@student.gsu.edu

**Rajshekhar Sunderraman**  
Dept. of Computer Science  
Georgia State University  
Atlanta, GA 30303  
rsunderraman@gsu.edu

**Shihao Ji\***  
School of Computing  
University of Connecticut  
Storrs, CT 06269  
shihao.ji@uconn.edu

## Abstract

Unmanned Aerial Vehicles (UAVs), equipped with cameras, are employed in numerous applications, including aerial photography, surveillance, and agriculture. In these applications, robust object detection and tracking are essential for the effective deployment of UAVs. However, existing benchmarks for UAV applications are mainly designed for traditional 2D perception tasks, restricting the development of real-world applications that require a 3D understanding of the environment. Furthermore, despite recent advancements in single-UAV perception, limited views of a single UAV platform significantly constrain its perception capabilities over long distances or in occluded areas. To address these challenges, we introduce UAV3D – a benchmark designed to advance research in both 3D and collaborative 3D perception tasks with UAVs. UAV3D comprises 1,000 scenes, each of which has 20 frames with fully annotated 3D bounding boxes on vehicles. We provide the benchmark for four 3D perception tasks: single-UAV 3D object detection, single-UAV object tracking, collaborative-UAV 3D object detection, and collaborative-UAV object tracking. Our dataset and code are available at [https://huiyegit.github.io/UAV3D\\_Benchmark/](https://huiyegit.github.io/UAV3D_Benchmark/).

## 1 Introduction

Due to their superior mobility, Unmanned Aerial Vehicles (UAVs) are widely deployed and crucially important in advancing numerous applications of computer vision, such as traffic monitoring, precision agriculture, disaster management, and wildlife surveillance, offering more efficiency and adaptability than traditional surveillance cameras with fixed perspectives. On the other hand, the availability of large-scale public datasets and benchmarks, such as ImageNet Deng et al. [2009] and MSCOCO Lin et al. [2014], has significantly accelerated progress of various computer vision tasks, including image classification, object detection, object tracking, semantic segmentation, and instance segmentation.

3D perception plays an essential role in vision-based robotic systems, enabling them to handle complex tasks beyond the capabilities of 2D perception. While still a relatively new technology for UAVs, 3D vision offers the ability to capture complete dimensional data of objects in a 3D environment. Currently, most UAV datasets Du et al. [2018], Zhu et al. [2018] are mainly designed for 2D perception, limiting the development of real-world applications that require 3D understanding of the surrounding environment. To bridge this gap, we introduce UAV3D to advance the research in 3D perception with UAVs.

Furthermore, despite recent advancements in single-UAV perception, limited views of a single UAV platform significantly constrain its perception capabilities over long distances or in occluded areas. A

---

\*Part of the work was done while the author was affiliated with Georgia State University.

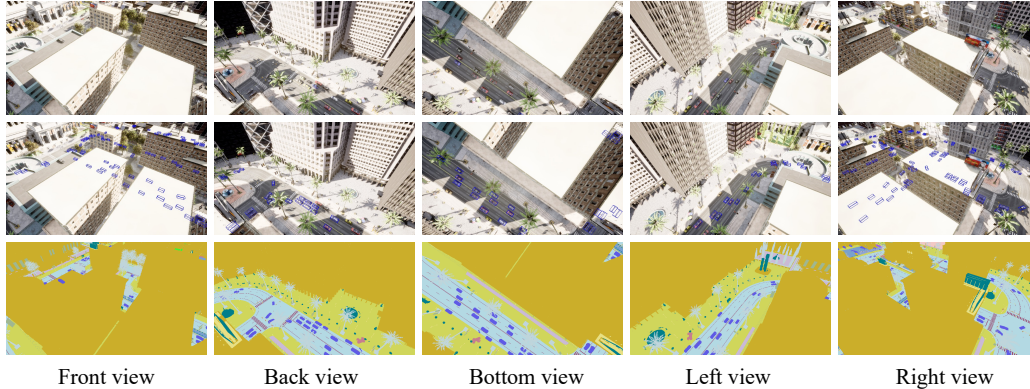


Figure 1: An example from the UAV3D dataset. From the top to bottom, they are 5 different RGB images from different camera views, images with 3D bounding boxes, and images with semantic labels.

promising solution lies in UAV-to-UAV communication, a cutting-edge technology that facilitates collaborative information exchange among UAVs. While there are several recent collaborative perception datasets Hao et al. [2024], Xu et al. [2023], Yu et al. [2022], Li et al. [2022], Xu et al. [2022b] for autonomous driving, there remains a noticeable gap of well-developed and organized collaborative perception datasets specifically for UAVs. Operating multiple UAVs simultaneously to build such a dataset is extremely challenging due to the high costs and extensive labor involved. Therefore, we focus on the development of a simulated dataset UAV3D to advance the research of collaborative perception for UAVs.

To create the UAV3D dataset, we utilize CARLA Dosovitskiy et al. [2017], a popular open-source simulator for autonomous driving, along with AirSim Shah et al. [2018] to simulate flying UAVs. The camera sensors mounted on UAVs are recorded synchronously to facilitate collaborative perception. In addition, diverse annotations, including bounding boxes, vehicle trajectories, and semantic labels are provided to support various downstream tasks. Figure 1 shows an example from the UAV3D dataset. To better support multi-UAV and multi-task perception research for UAVs, we further provide the benchmarks for four 3D perception tasks, including single-UAV 3D object detection, single-UAV object tracking, collaborative-UAV 3D object detection, and collaborative-UAV object tracking.

## 2 Related work

Over the past few years, several datasets have been developed to advance the perception tasks in autonomous driving and UAVs. The UAVDT Du et al. [2018] dataset comprises 100 video sequences selected from more than 10 hours of footage captured by a UAV platform across various urban locations. The VisDrone Zhu et al. [2018] dataset includes 263 video clips, comprising 179k frames and 10k static images, captured by diverse drone-mounted cameras from multiple locations and weather conditions. However, both benchmarks are small-scale, real-world datasets designed for 2D perception tasks. In contrast, our UAV3D is a large-scale simulated dataset, comprising 500k images for 3D perception tasks. The Waymo Open Sun et al. [2020] and nuScenes Caesar et al. [2020] datasets are two public, large-scale, multi-modal datasets that include camera, radar, and lidar data for autonomous driving. Our UAV3D comprises 1,000 scenes, matching the scale of the nuScenes dataset. It also has the same format as nuScenes to provide annotations and metadata, such as calibration, maps, and vehicle coordinates. OPV2V Xu et al. [2022b], V2X-Sim Li et al. [2022], and V2XSet Xu et al. [2022a] are three simulated multi-agent perception datasets designed for V2X-aided autonomous driving. OPV2V supports multi-modal data and multi-agent collaborative perception in a vehicle-to-vehicle scenario. Meanwhile, V2X-Sim and V2XSet provide multi-agent sensor recordings from roadside units (RSUs) and multiple vehicles, enabling collaborative perception in both vehicle-to-vehicle and vehicle-to-roadside scenarios. Our UAV3D utilizes the same baseline models as V2X-Sim to evaluate the collaborative perception tasks for UAVs. CoPerception-UAV Hu et al. [2022] is a simulated dataset for UAV-based collaborative perception, featuring 131.9k synchronous images captured at three different altitudes across three towns and in two swarm formations. In comparison,

Table 1: Comparison of recent related datasets for autonomous driving and UAVs. Real and Sim refer to real-world and simulated dataset, respectively. V2X, V2V and V2I denote the vehicle-to-everything, vehicle-to-vehicle and vehicle-to-infrastructure cooperation, respectively. C, L and R refer to Camera, Lidar and Radar sensor, respectively. While CoPerception-UAV includes vehicles with 21 different categories, UAV3D has 17 different categories of vehicles.

Dataset	Year	Real/sim	Scenario	V2X	Modality	Scenes	Frames	Images	3D boxes	Classes
VisDrone Zhu et al. [2018]	2018	Real	Drone	No	C	–	179.2K	10.2K	No	10
UAVDT Du et al. [2018]	2018	Real	Drone	No	C	–	80K	80K	No	3
Waymo Open Sun et al. [2020]	2019	Real	Driving	No	C & L	1K	200K	1M	12M	4
nuScenes Caesar et al. [2020]	2019	Real	Driving	No	C & L & R	1K	40K	1.4M	1.4M	23
OPV2V Xu et al. [2022b]	2022	Sim	Driving	V2V	C & L	–	–	44K	230K	1
V2X-Sim Li et al. [2022]	2022	Sim	Driving	V2X	C & L	–	–	60K	26.6K	1
V2XSet Xu et al. [2022a]	2022	Sim	Driving	V2X	C & L	–	–	44K	230K	1
DAIR-V2X Yu et al. [2022]	2022	Real	Driving	V2I	C & L	–	–	39K	464K	10
CoPerception-UAV Hu et al. [2022]	2022	Sim	Drone	V2V	C	183	4.4K	131.9K	1.6M	21
V2V4Real Xu et al. [2023]	2023	Real	Driving	V2V	C & L	–	–	40K	240K	5
Rcooper Hao et al. [2024]	2024	Real	Driving	V2I	C & L	–	–	50K	–	10
TUMTraf-V2X Zimmer et al. [2024]	2024	Real	Driving	V2I	C & L	–	–	5K	29.3K	8
HoloVIC Ma et al. [2024]	2024	Real	Driving	V2I	C & L	–	100K	–	11.4M	3
V2X-Real Xiang et al. [2024]	2024	Real	Driving	V2X	C & L	–	–	171K	1.2M	10
UAV3D	2024	Sim	Drone	V2V	C	1K	20K	500K	3.3M	17

our UAV3D contains 500k images captured over four diverse towns, making it approximately four times larger in scale than CoPerception-UAV. DAIR-V2X Yu et al. [2022], V2V4Real Xu et al. [2023], Rcooper Hao et al. [2024], TUMTraf-V2X Zimmer et al. [2024], HoloVIC Ma et al. [2024] and V2X-Real Xiang et al. [2024] are six large-scale, real-world datasets that facilitate vehicle-centric collaborative perception for autonomous driving, each emphasizing different cooperative scenarios: vehicle-to-infrastructure cooperation in DAIR-V2X, vehicle-to-vehicle cooperation in V2V4Real, vehicle-to-roadside cooperation in Rcooper, vehicle-to-infrastructure cooperation in TUMTraf-V2X, vehicle-to-infrastructure cooperation in HoloVIC, vehicle-to-vehicle and vehicle-to-infrastructure cooperation in V2X-Real. In contrast, UAV3D is a large-scale simulation dataset designed to support UAV-centric collaborative perception, specifically focusing on UAV-to-UAV cooperation scenario. The comparison of related datasets is summarized in Table 1.

### 3 Benchmark Dataset

#### 3.1 Data Collection

**CARLA-AirSim Co-simulation.** We utilize the open-source CARLA Dosovitskiy et al. [2017] and AirSim Shah et al. [2018] simulators for traffic flow simulation and data recording. In CARLA, vehicles are spawned to navigate randomly throughout the town. Hundreds of vehicles (i.e., 200) are active in each town (Town 3, 6, 7, and 10), which feature complex traffic situations, such as crossroads and T-junctions. We record 250 log files per town, resulting in a total of 1,000 scenes.

**Flight Planning.** We operate UAVs in Towns 3, 6, 7, and 10 of CARLA, with Town 10 being particularly known for its dense traffic and highly challenging driving situations. We emphasize the variations between urban (Towns 3 and 10) and suburban (Towns 6 and 7) settings, particularly in terms of traffic flow, vegetation, architecture, vehicles, and road markings. For each town in CARLA, we have established 25 flight routes to cover a diverse range of locations from the bottom left to the top right of the map.

**Sensor Setup.** As shown in Figure 2, we equip each UAV with five RGB cameras to capture both RGB and semantic images. Four of these cameras face the front, left, right, and back with a pitch angle of -45 degree, while the bottom camera provides a bird’s eye view. The resolution of the images is 800x450 pixels. CARLA uses the Unreal Engine (UE) coordinate system, with x-forward, y-right, and z-up, returning coordinates in local space. AirSim, on the other hand, adopts the North-East-Down (NED) coordinate system, where north aligns with the Unreal Engine x-axis. We adjust the sensor coordinates from AirSim to align with vehicle coordinates from CARLA.

**UAV-Swarm Formation.** As shown in Figure 3, we configure a swarm of five UAVs in a cross-shaped formation with the positions at the front, left, right, center, and back, each with a 20-meter distance from the center UAV. The swarm of UAVs maintains the formation, while performing perception and collaboration tasks at an altitude of 60 meters.

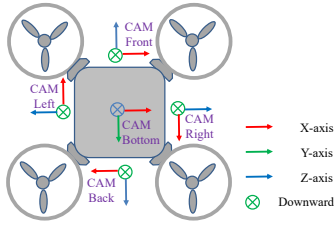


Figure 2: Sensor setup for our data collection platform.

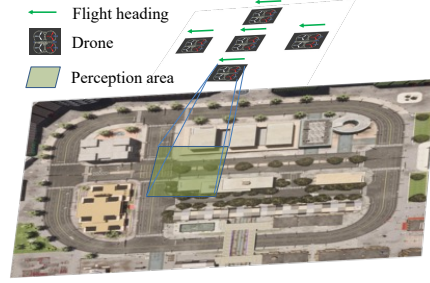


Figure 3: UAV swarm with a cross-shaped formation.

### 3.2 Coordinate Systems

**Global Coordinate System.** The nuScenes dataset uses the East-North-Up (ENU) coordinate system for its global frame. The ENU system is a right-handed Cartesian coordinate system, where the X-axis points to the East, the Y-axis points to the North, and the Z-axis points upward. This system provides a stable, global reference frame for objects and vehicle locations across different scenes in nuScenes. In contrast, the UAV3D dataset, utilizing Unreal Engine 4 (UE4), employs a left-handed Cartesian coordinate system commonly used in real-time rendering and 3D graphics environments. In this system, the X-axis points forward, the Y-axis points to the right, and the Z-axis points upward, following the left-handed rule. Table 2 shows the comparison of the global coordinate systems between nuScenes and UAV3D.

Table 2: Comparison of the global coordinate systems between nuScenes and UAV3D.

	nuScenes (ENU)	UAV3D (Unreal Engine 4)
Type	Right-handed	Left-handed
X-axis	Point to East	Point Forward
Y-axis	Point to North	Point to Right
Z-axis	Point Up	Point Up
Application	Autonomous driving, real-world mapping	3D rendering for games, simulations

**Ego-UAV Coordinate System.** In UAV3D, the Ego-UAV coordinate system is aligned with the global coordinate system in Unreal Engine 4, and they share the same origin and orientation of the X, Y, and Z axes. This setup simplifies transformations between UAV’s local reference frame and the global environment, ensuring consistency in positioning and orientation throughout the dataset.

**Camera Coordinate System.** The camera coordinate system is a 3D coordinate system that describes the position of an object relative to the camera, where the X-axis points to the right of the camera, Y-axis points downwards and Z-axis points forward, away from the camera, representing the depth of an object in the scene. The transformation from world coordinate  $\mathbf{P}_w$  to camera coordinate  $\mathbf{P}_c$  can be expressed using the following equation:

$$\mathbf{P}_c = \begin{bmatrix} \mathbf{R} & \mathbf{T} \\ \mathbf{0} & 1 \end{bmatrix} \cdot \mathbf{P}_w, \quad (1)$$

where  $\mathbf{P}_c = [x_c, y_c, z_c, 1]^T$  is the camera coordinate point,  $\mathbf{R}$  is a 3x3 rotation matrix,  $\mathbf{T}$  is a 3x1 translation vector, and  $\mathbf{P}_w = [x_w, y_w, z_w, 1]^T$  represents the homogeneous coordinates in the world coordinate system. To transform from Unreal Engine 4 (left-handed) to the standard coordinate system (right-handed), the axes need to be rotated and flipped. As a result, a point  $(x, y, z)$  in the left-handed system is transformed into the right-handed system as  $(x, y, z) \rightarrow (y, -z, x)$ . In UAV3D, the transformation from world coordinate  $\mathbf{P}_w$  to camera coordinate  $\mathbf{P}'_c$  can be expressed as follows:

$$\mathbf{P}'_c = \begin{bmatrix} 0 & 1 & 0 & 0 \\ 0 & 0 & -1 & 0 \\ 1 & 0 & 0 & 0 \\ 0 & 0 & 0 & 1 \end{bmatrix} \cdot \mathbf{P}_c = \begin{bmatrix} 0 & 1 & 0 & 0 \\ 0 & 0 & -1 & 0 \\ 1 & 0 & 0 & 0 \\ 0 & 0 & 0 & 1 \end{bmatrix} \cdot \begin{bmatrix} \mathbf{R} & \mathbf{T} \\ \mathbf{0} & 1 \end{bmatrix} \cdot \mathbf{P}_w, \quad (2)$$

where  $\mathbf{P}'_c = [x'_c, y'_c, z'_c, 1]^T$ .

**Pixel Coordinates.** Pixel coordinates refer to the 2D coordinates  $(u, v)$  on an image plane, representing the location of a point in the image as captured by a camera. The transformation from the 3D camera coordinates  $(x'_c, y'_c, z'_c)^T$  to the 2D pixel coordinates  $(u, v)$  is typically done using the camera intrinsic matrix. The intrinsic matrix accounts for properties of the camera, such as focal length and the optical center of the image. The transformation is formulated as:

$$\begin{bmatrix} u \\ v \\ 1 \end{bmatrix} = \begin{bmatrix} f_x & 0 & c_x \\ 0 & f_y & c_y \\ 0 & 0 & 1 \end{bmatrix} \cdot \begin{bmatrix} \frac{x'_c}{z'_c} \\ \frac{y'_c}{z'_c} \\ 1 \end{bmatrix}, \quad (3)$$

where  $(u, v)$  are the corresponding pixel coordinates,  $f_x, f_y$  are the focal lengths of the camera along the  $x$  and  $y$  axes, and  $c_x, c_y$  are center coordinates in the image plane.

### 3.3 Image Data and Annotation

We collect synchronous images from all cameras mounted on the five UAVs, totaling 25 images per sample. To support downstream tasks (e.g., detection, tracking, and semantic segmentation), we extract vehicle annotations from the CARLA simulator, and the camera intrinsics and extrinsics from the AirSim simulator. We offer various annotations, including 3D bounding boxes, and pixel-wise semantic labels. Each 3D bounding box is defined by the location of its center in  $x, y$ , and  $z$  coordinates, along with dimensions of width, length, height, and orientation angles (yaw, pitch, roll). UAV3D comprises 500k images and 3.3 million 3D bounding boxes, divided into training, validation, and test splits. There are 17 vehicle categories in the dataset, which is organized in a similar format as the popular nuScenes dataset, with the compatibility to the well-established nuScenes-devkit.

## 4 Experiments

We benchmark four standard perception tasks for UAVs: single-UAV 3D object detection, single-UAV object tracking, collaborative-UAV 3D object detection, and collaborative-UAV object tracking. These tasks are essential for the broad applications of UAVs in various fields. For performance evaluations of the four perception tasks, we utilize the same metrics as those used in the Nuscenes Caesar et al. [2020] dataset.

**Dataset Format and Split.** Our UAV3D dataset adopts the format of nuScenes. Each scene in our dataset consists of 20 frames. In each scene, 5 UAVs are selected as the collaborating agents, and each frame features data sampled from 5 UAVs. We generate 1,000 scenes, totaling 20,000 frames, from which 700 scenes are used for training, 150 for validation, and 150 for test. Consequently, our dataset comprises 14,000 samples in the training set, 3,000 samples in the validation set, and 3,000 samples in the test set.

**Implementation Details.** The bird’s-eye view (BEV), a compact 2D map that accurately describes surrounding objects, is a widely used and effective representation in 3D perception. We therefore employ BEV-based representations across all four tasks. We map all vehicle classes to a single “car” class for the perception tasks. However, the original 17 categories are available for more fine-grained perception tasks. We set the perception range of  $[-102.4\text{m}, 102.4\text{m}]$  for the X-axis and  $[-102.4\text{m}, 102.4\text{m}]$  for the Y-axis, defined in the Ego-UAV Euclidean coordinate system. All baseline models were trained with a batch size of 4 for 24 epochs, with a per-GPU batch size of 1. All experiments were conducted on a computing server equipped with 8 Nvidia A100 GPUs.

**Benchmark Models.** For the single-UAV perception tasks, we consider three recent works in autonomous driving, including PETR Liu et al. [2022, 2023b], BEVFusion Liu et al. [2023c], and DETR3D Wang et al. [2022]. PETR Liu et al. [2022] transforms multi-view 2D features into 3D position-aware features by incorporating a 3D positional embedding. The object queries, initialized from 3D space, can directly perceive the 3D object information by interacting with the produced 3D position-aware features. In our implementation of PETR on UAV3D, we experimented with both ResNet-50 and ResNet-101 as backbones. However, PETR’s performance with ResNet-101 was inferior to that with ResNet-50. We chose not to include this unexpected result in the paper, as ResNet-101 typically outperforms ResNet-50. Consequently, we adopted only ResNet-50 as the backbone for the PETR baseline.

Table 3: 3D object detection results on the **validation** set of UAV3D. The best results among all the methods are in bold. The symbol "\*" denotes that we have rounded the original value of mAOE from BEVFusion to 1.0.

Method	Backbone	Size	mAP $\uparrow$	NDS $\uparrow$	mATE $\downarrow$	mASE $\downarrow$	mAOE $\downarrow$
PETR Liu et al. [2022]	Res-50	704 $\times$ 256	0.512	0.571	0.741	0.173	0.072
BEVFusion Liu et al. [2023c]	Res-50	704 $\times$ 256	0.487	0.458	0.615	<b>0.152</b>	1.000*
DETR3D Wang et al. [2022]	Res-50	704 $\times$ 256	0.430	0.509	0.791	0.187	0.100
PETR Liu et al. [2022]	Res-50	800 $\times$ 450	0.581	0.632	0.625	0.160	<b>0.064</b>
BEVFusion Liu et al. [2023c]	Res-101	800 $\times$ 450	0.536	0.582	0.521	0.154	0.343
DETR3D Wang et al. [2022]	Res-101	800 $\times$ 450	<b>0.618</b>	<b>0.671</b>	<b>0.494</b>	0.158	0.070

BEVFusion Liu et al. [2023c] is a generic multi-task multi-sensor perception framework, which performs sensor fusion in a shared BEV space and treats foreground, background, geometric and semantic information equally. Since UAV3D contains RGB images without other modality data, we utilize BEVFusion to process the RGB-modality only. DETR3D Wang et al. [2022] projects learnable 3D queries in 2D images, and then samples the corresponding features for end-to-end 3D bounding box prediction without NMS post-processing.

For the collaborative-UAV perception tasks, we consider four collaboration algorithms as the benchmark models, including When2Com Liu et al. [2020a], Who2Com Liu et al. [2020b], V2VNet Wang et al. [2020], and DiscoNet Li et al. [2021], all of which have different communication strategies to transmit and fuse the intermediate features. Lower-bound is the single-UAV perception model without collaboration from other agents. Upper-bound is the collaboration model which transmits the raw image data to other agents. While this approach fully leverages the available perception data, it requires a large amount of transmission bandwidth. As for the implementation of the upper-bound baseline, the 25 images from 5 UAVs are directly utilized by the BEVFusion model.

When2Com Liu et al. [2020a] employs attention-based mechanism for communication group construction: the agents with high correlation scores would be selected as the collaborators. After the attention-based fusion, the updated features would be fed into model head for perception prediction. Who2Com Liu et al. [2020b] has a similar communication method with When2Com, but it employs a handshake mechanism to select the agent with the highest attention score. V2VNet Wang et al. [2020] utilizes a graph neural network to propagate the information within the agents, and employs a convolutional gated recurrent module to fuse the information from other agents. After several rounds of neural message passing, the updated features are fed into the model head to generate perception results. DiscoNet Li et al. [2021] utilizes a directed collaboration graph with matrix-valued edge weight to adaptively choose the informative spatial regions and reject the noisy regions of image features sent by other agents. After the message fusion, the updated features would be transmitted to the model head for perception results.

#### 4.1 Single-UAV 3D Object Detection

**Problem Definition.** As one of the most critical perception tasks for UAVs, 3D object detection is designed to localize and recognize objects in 3D space using a single frame. Subsequent tracking tasks depend heavily on the accuracy of these detection results. The models for this task process images from five different perspectives and generate predictions of 3D bounding boxes.

**Backbone and Evaluation.** For the three benchmark models, namely PETR, BEVFusion, and DETR3D, we utilize two backbone architectures, ResNet-50 and ResNet-101, with two different image sizes: (704, 256) and (800, 450). We apply the BEV detection evaluation metrics as used in nuScenes, including NDS, mAP, mATE, mASE, and mAOE. The definitions of these metrics are the same as in Nuscenes Caesar et al. [2020]. Compared to nuScenes, we do not include the mAVE and mAAE metrics. Therefore, NDS is defined as follows:

$$\text{NDS} = \frac{1}{8} [5 \text{ mAP} + \sum_{\text{mTP} \in \mathbb{TP}} (1 - \min(1, \text{mTP}))], \quad (4)$$

where  $\mathbb{TP}$  is a set of the three mean True Positive metrics: mATE, mASE, and mAOE. We focus on analyzing the detection results and report them for both validation and test sets.

**Quantitative Results.** Table 3 reports the results of 3D object detection. Among the three baselines, DETR3D achieves the best detection results in three of five metrics, including mAP, NDS and mATE.

Table 4: 3D object detection results on the **test** set of UAV3D. The best results among all the methods are in bold. The symbol "\*" has the same meanings as in Table 3.

Method	Backbone	Size	mAP $\uparrow$	NDS $\uparrow$	mATE $\downarrow$	mASE $\downarrow$	mAOE $\downarrow$
PETR Liu et al. [2022]	Res-50	704 $\times$ 256	0.507	0.568	0.748	0.173	0.069
BEVFusion Liu et al. [2023c]	Res-50	704 $\times$ 256	0.485	0.456	0.619	0.153	1.000*
DETR3D Wang et al. [2022]	Res-50	704 $\times$ 256	0.424	0.505	0.794	0.187	0.094
PETR Liu et al. [2022]	Res-50	800 $\times$ 450	0.575	0.627	0.632	0.159	<b>0.061</b>
BEVFusion Liu et al. [2023c]	Res-101	800 $\times$ 450	0.536	0.583	0.518	<b>0.156</b>	0.339
DETR3D Wang et al. [2022]	Res-101	800 $\times$ 450	<b>0.610</b>	<b>0.665</b>	<b>0.501</b>	0.157	0.068

Table 5: Object tracking results on the **validation** set of UAV3D. The best results among all the methods are in bold.

Method	Backbone	Size	AMOTA $\uparrow$	AMOTP $\downarrow$	MOTA $\uparrow$	MOTP $\downarrow$	TID $\downarrow$	LGD $\downarrow$
			(%)	(m)	(%)	(m)	(s)	(s)
PETR Liu et al. [2022]	Res-50	704 $\times$ 256	0.199	1.294	0.195	0.794	1.280	2.970
BEVFusion Liu et al. [2023c]	Res-50	704 $\times$ 256	0.566	1.137	0.501	0.695	0.790	1.600
DETR3D Wang et al. [2022]	Res-50	704 $\times$ 256	0.089	1.382	0.121	0.800	1.540	3.530
PETR Liu et al. [2022]	Res-50	800 $\times$ 450	0.291	1.156	0.256	0.677	1.090	2.550
BEVFusion Liu et al. [2023c]	Res-101	800 $\times$ 450	<b>0.606</b>	<b>1.006</b>	<b>0.540</b>	0.627	<b>0.700</b>	<b>1.390</b>
DETR3D Wang et al. [2022]	Res-101	800 $\times$ 450	0.262	1.123	0.238	<b>0.561</b>	1.140	2.720

The results of the three baselines are comparable in terms of mASE, although BEVFusion performs slightly better than the other two baselines. In terms of mAOE, PETR and DETR3D significantly outperform BEVFusion. On the other hand, using larger backbones and input sizes can significantly enhance baseline performance. For instance, DETR3D shows substantial improvements, with gains of approximately 0.18 in mAP and 0.16 in NDS. Meanwhile, BEVFusion has the modest increases, with gains of about 0.05 in mAP and 0.13 in NDS. Table 4 presents the results of 3D object detection on the test set, which are consistent with those observed on the validation set.

## 4.2 Single-UAV Object Tracking

**Problem Definition.** Unlike the object detection, the object tracking requires the production of temporally consistent perception results. In this task, object tracking involves utilizing bounding boxes and object identities to track various objects across a temporal sequence.

**Evaluation Metrics.** We employ the object tracking evaluation metrics defined in nuScenes Caesar et al. [2020], including Average Multi Object Tracking Accuracy (AMOTA), Average Multi Object Tracking Precision (AMOTP), Track Initialization Duration (TID), and Longest Gap Duration (LGD). In addition, the traditional metrics are also employed, such as Object Tracking Accuracy (MOTA) and Object Tracking Precision (MOTP). While MOTA can measure detection errors and association errors, MOTP measures localization accuracy.

**Quantitative Results.** Table 5 reports the results of object tracking on the validation set. BEVFusion achieves the best tracking performance across five of six metrics, specifically AMOTA, AMOTP, MOTA, TID, and LGD, and achieves the second-best result in MOTP. The baselines PETR and DETR3D demonstrate comparable performances, yet they lag behind BEVFusion by a large margin, with a difference of approximately 0.3 in AMOTA. Similar to the single-UAV object detection task, the object tracking performance of the three baselines benefits from the use of larger backbones and input image sizes. DETR3D achieves significant improvements, with gains of approximately 0.18 in AMOTA and 0.11 in MOTA. In contrast, BEVFusion shows smaller increases, with about 0.04 in AMOTA and 0.04 in MOTA. Table 6 shows the results of object tracking on test set, which are consistent with those observed on the validation set.

## 4.3 Collaborative-UAV 3D Object Detection

**Problem Definition.** Similar to single-UAV 3D object detection, the objective of collaborative-UAV 3D object detection is to localize and recognize objects in 3D space using a single frame. However, in collaborative-UAV 3D object detection, one agent can collaborate with other agents to enhance perception performance.

**Model and Evaluation.** We employ the BEVFusion with backbone Swin-transformer Liu et al. [2021] as the basic framework, and incorporate different communication strategies to the benchmark,

Table 6: Single-UAV object tracking results on the **test** set of UAV3D. The best results among all the methods are in bold.

Method	Backbone	Size	AMOTA $\uparrow$	AMOTP $\downarrow$	MOTA $\uparrow$	MOTP $\downarrow$	TID $\downarrow$	LGD $\downarrow$
			(%)	(m)	(%)	(m)	(s)	(s)
PETR Liu et al. [2022]	Res-50	704 $\times$ 256	0.198	1.295	0.193	0.792	1.300	2.940
BEVFusion Liu et al. [2023c]	Res-50	704 $\times$ 256	0.561	1.140	0.494	0.701	0.790	1.580
DETR3D Wang et al. [2022]	Res-50	704 $\times$ 256	0.091	1.382	0.122	0.801	1.590	3.610
PETR Liu et al. [2022]	Res-50	800 $\times$ 450	0.288	1.157	0.252	0.681	1.13	2.61
BEVFusion Liu et al. [2023c]	Res-101	800 $\times$ 450	<b>0.600</b>	<b>1.039</b>	<b>0.533</b>	0.615	<b>0.710</b>	<b>1.440</b>
DETR3D Wang et al. [2022]	Res-101	800 $\times$ 450	0.259	1.125	0.238	<b>0.563</b>	1.190	2.730

Table 7: Collaborative-UAV 3D object detection results on the **validation** set of UAV3D. The best results among all the methods are in bold.

Method	mAP $\uparrow$	NDS $\uparrow$	mATE $\downarrow$	mASE $\downarrow$	mAOE $\downarrow$
Lower-bound	0.544	0.556	0.540	0.147	0.578
When2Com Liu et al. [2020a]	0.550	0.507	0.534	0.156	0.679
Who2Com Liu et al. [2020b]	0.546	0.597	0.541	0.150	0.263
V2VNet Wang et al. [2020]	0.647	0.628	0.508	0.167	0.533
DiscoNet Li et al. [2021]	0.700	0.689	0.423	0.143	0.422
Upper-bound	<b>0.720</b>	<b>0.748</b>	<b>0.391</b>	<b>0.106</b>	<b>0.117</b>

Table 8: Collaborative-UAV 3D object detection results on the **test** set of UAV3D. The best results among all the methods are in bold.

Method	mAP $\uparrow$	NDS $\uparrow$	mATE $\downarrow$	mASE $\downarrow$	mAOE $\downarrow$
Lower-bound	0.542	0.558	0.543	0.148	0.549
When2Com Liu et al. [2020a]	0.547	0.505	0.539	0.156	0.659
Who2Com Liu et al. [2020b]	0.541	0.594	0.548	0.150	0.255
V2VNet Wang et al. [2020]	0.645	0.626	0.517	0.166	0.527
DiscoNet Li et al. [2021]	0.696	0.686	0.428	0.143	0.417
Upper-bound	<b>0.720</b>	<b>0.746</b>	<b>0.398</b>	<b>0.107</b>	<b>0.121</b>

including Lower-bound, When2Com Liu et al. [2020a], Who2Com Liu et al. [2020b], V2VNet Wang et al. [2020], DiscoNet Li et al. [2021], and Upper-bound. We employ the 3D object detection metrics as in nuScenes: NDS, mAP, mATE, mASE, and mAOE. We target the detection results and report them on the validation and test sets.

**Quantitative Results.** Table 7 reports the results of collaborative-UAV 3D object detection on validation set. The Upper-bound baseline has achieved the best performance and outperformed the Lower-bound baseline by a large gap of 0.18 in mAP and 0.19 in NDS because the Upper-bound baseline can fully utilize the perception image data from all the five collaborative UAVs. DiscoNet has achieved the best performance in the four collaborative baselines, with a slight performance gap of 0.02 in mAP and 0.06 in NDS, compared to the Upper-bound. V2VNet has the second best performance due to the effective fusion of image features. The When2Com and Who2Com baselines have slightly better performance than the Lower-bound baseline since the fusion mechanism can only choose parts of intermediate image features from other agents. Specifically, When2Com has a threshold score to filter out the image features with low attention score, while Who2Com chooses the image features with the largest attention score from one of the collaborative agents. Table 8 reports the results of collaborative-UAV 3D object detection on test set, which again are consistent with those observed on the validation set.

#### 4.4 Collaborative-UAV Object Tracking

**Problem Definition.** Similar to single-UAV object tracking, the objective of collaborative-UAV object tracking is to use bounding boxes, and object identities to track different objects within a temporal sequence. However, in collaborative-UAV 3D object tracking, one agent can collaborate with other agents to boost the tracking performance.

**Model and Evaluation.** Following the collaborative-UAV 3D object detection, we employ the BEVFusion with backbone Swin-transformer Liu et al. [2021] as the basic framework, and incorporate different communication strategies to the benchmarks, including Lower-bound, When2Com Liu et al. [2020a], Who2Com Liu et al. [2020b], V2VNet Wang et al. [2020], DiscoNet Li et al. [2021], and



Table 9: Collaborative-UAV object tracking results on the **validation** set of UAV3D. The best results among all the methods are in bold.

Method	AMOTA $\uparrow$	AMOTP $\downarrow$	MOTA $\uparrow$	MOTP $\downarrow$	TID $\downarrow$	LGD $\downarrow$
	(%)	(m)	(%)	(m)	(s)	(s)
Lower-bound	0.644	1.018	0.593	0.611	0.620	1.280
When2Com Liu et al. [2020a]	0.646	1.012	0.595	0.618	0.590	1.200
Who2Com Liu et al. [2020b]	0.648	1.012	0.602	0.623	0.580	1.200
V2VNet Wang et al. [2020]	0.782	0.803	0.735	0.587	0.360	0.710
DiscoNet Li et al. [2021]	0.809	0.703	0.766	0.516	0.300	0.590
Upper-bound	<b>0.812</b>	<b>0.672</b>	<b>0.781</b>	<b>0.476</b>	<b>0.300</b>	<b>0.570</b>

Table 10: Collaborative-UAV object tracking results on the **test** set of UAV3D. The best results among all the methods are in bold.

Method	AMOTA $\uparrow$	AMOTP $\downarrow$	MOTA $\uparrow$	MOTP $\downarrow$	TID $\downarrow$	LGD $\downarrow$
	(%)	(m)	(%)	(m)	(s)	(s)
Lower-bound	0.641	1.020	0.590	0.614	0.610	1.270
When2Com Liu et al. [2020a]	0.643	1.016	0.591	0.611	0.610	1.250
Who2Com Liu et al. [2020b]	0.645	1.017	0.597	0.631	0.600	1.220
V2VNet Wang et al. [2020]	0.778	0.811	0.727	0.598	0.360	0.710
DiscoNet Li et al. [2021]	0.807	0.707	0.760	0.512	0.330	0.650
Upper-bound	<b>0.810</b>	<b>0.679</b>	<b>0.772</b>	<b>0.485</b>	<b>0.300</b>	<b>0.580</b>

Upper-bound. Regarding the evaluation metrics, we employ AMOTA, AMOTP, MOTA, MOTP, TID, and LGD as those used in the single-UAV object tracking task.

**Quantitative Results.** Table 9 reports the results of collaborative-UAV object tracking on the validation set. The Upper-bound baseline has shown a large performance gain against the Lower-bound baseline by about 0.17 in AMOTA and 0.44 in AMOTP, which demonstrates the effectiveness of collaborative perception for utilizing image data from other UAVs. DiscoNet has achieved the best performance in the four intermediate feature fusion baselines, with a large performance improvement of 0.16 in AMOTA and 0.31 in AMOTP, compared to the Low-bound. V2VNet has the second-best performance among the four baselines due to the effective fusion of image features. The When2Com and Who2Com baselines have shown better performance than Lower-bound due to the attention mechanism for fusing intermediate image features from other agents. Table 10 shows the results of collaborative-UAV object tracking on the test set, which are consistent with those observed on the validation set.

#### 4.5 Visualization

Figure 4 presents the qualitative results of 3D object detection of the six collaborative baselines in the challenging urban environment of Town 10. As shown in Figure 4(a), the Lower-bound model

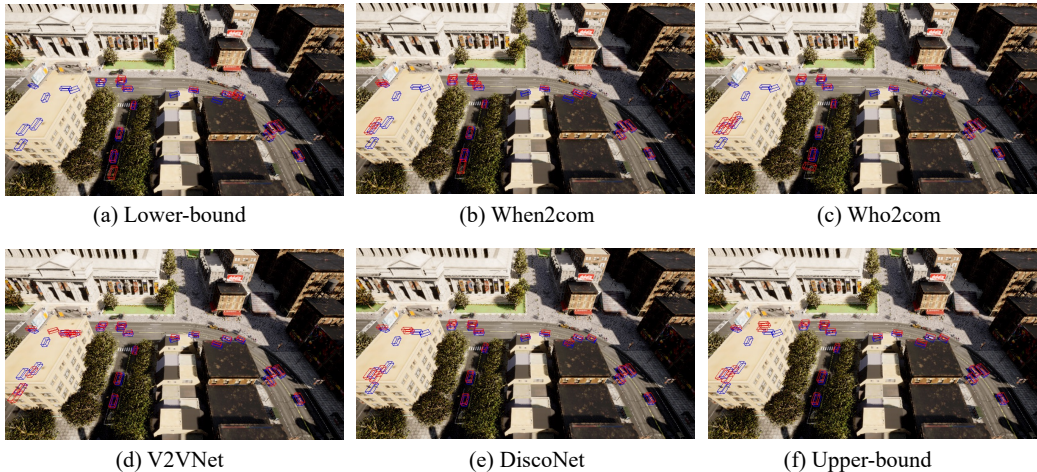


Figure 4: Visualization of the **back view** for collaborative-UAV 3D object detection results on UAV3D. Red boxes represent the predictions, while blue boxes indicate the ground truth.

exhibits relatively lower detection performance in terms of bounding box size and orientation, and it fails to predict objects obstructed by tall buildings due to the occlusions. Figure 4(f) illustrates that the predicted 3D bounding boxes (in red) generated by the Upper-bound baseline closely align with the ground truth annotations (in blue) in terms of box size and orientation. Notably, the Upper-bound model successfully detects vehicles even when they are obscured by tall buildings. This illustrates the effectiveness of collaborative perception in overcoming occlusions in complex urban environments. Regarding some failure cases, certain missing bounding boxes fall outside the detection range specified in our settings. Additionally, there remains substantial room of improvement for advanced model designs. The four intermediate feature fusion methods outperform the Lower-bound baseline, demonstrating the capability to detect objects obscured by tall buildings. Among the four baselines, When2Com and Who2Com exhibit relatively lower performance, while DiscoNet has demonstrated the best performance, with the detection results closely aligned with those of the Upper-bound baseline. Visualizations of the front, bottom, left, and right views can be found in the Appendix.

## 5 Limitations

Real-world datasets typically involve more complex conditions, including localization errors, sensor synchronization issues, and communication latency between agents. In contrast, simulated datasets benefit from the controlled, ideal settings of a simulation environment. Apparently, there is a domain gap between the real and simulated datasets, where the performance would degrade when applying models trained with simulated data to the real-world applications. The typical approach to mitigate the domain gap is to the domain adaptation technique, which trains the model on the simulated dataset and adapt the model to real-world applications. To the best of our knowledge, the real-world 3D dataset for UAVs is not publicly available due to security, privacy concerns, and the expensive cost of data annotation. We can adapt the sim-to-real domain adaption algorithms in autonomous driving Xu et al. [2023], Li et al. [2024a] to the UAV3D dataset. Moreover, to evaluate perception tasks on UAV3D, we have selected three well-known baseline models from the autonomous driving community: BEVFusion, DETR3D, and PETR. Recently, several advanced models for 3D object detection in autonomous driving, such as StreamPETR Wang et al. [2023], Sparse4DV2 Lin et al. [2023], BEVNeXt Li et al. [2024b], and SparseBEV Liu et al. [2023a], have been proposed. These models can be adapted to UAV3D and potentially can achieve even better performance. We leave this exploration for future work.

## 6 Conclusion

We introduce UAV3D – a large-scale 3D perception benchmark for Unmanned Aerial Vehicles – collected from the CARLA-AirSim co-simulation environment. UAV3D features the largest collection of RGB images and 3D bounding-box annotations compared to previously released UAV datasets, and supports a wide range of 3D perception tasks. To facilitate UAV-related research, we have benchmarked several recent perception models from autonomous driving, adapting them to single-UAV object detection and tracking, and collaborative-UAV object detection and tracking. The whole benchmark, including the UAV3D dataset and source code, is made publicly available, with the aim to facilitate research in UAV-based 3D perception. Future work includes incorporating a diverse range of times (day and night) and weather conditions (sun, rain, and clouds) in the data collection, simulating latency issues, and exploring more advanced models for 3D perception. We believe our work will inspire many relevant research including but not limited to multi-agent reinforcement learning and collaborative learning systems.

## Acknowledgments and Disclosure of Funding

The software and data were created by Georgia State University Research Foundation under Army Research Laboratory (ARL) Award Numbers W911NF-22-2-0025 and W911NF-23-2-0224. ARL, as the Federal awarding agency, reserves a royalty-free, nonexclusive and irrevocable right to reproduce, publish, or otherwise use this software for Federal purposes, and to authorize others to do so in accordance with 2 CFR 200.315(b).

## References

- Holger Caesar, Varun Bankiti, Alex H Lang, Sourabh Vora, Venice Erin Liong, Qiang Xu, Anush Krishnan, Yu Pan, Giancarlo Baldan, and Oscar Beijbom. nuscenes: A multimodal dataset for autonomous driving. In *Proceedings of the IEEE/CVF conference on computer vision and pattern recognition*, pages 11621–11631, 2020.
- Jia Deng, Wei Dong, Richard Socher, Li-Jia Li, Kai Li, and Li Fei-Fei. Imagenet: A large-scale hierarchical image database. In *2009 IEEE conference on computer vision and pattern recognition*, pages 248–255. Ieee, 2009.
- Alexey Dosovitskiy, German Ros, Felipe Codevilla, Antonio Lopez, and Vladlen Koltun. Carla: An open urban driving simulator. In *Conference on robot learning*, pages 1–16. PMLR, 2017.
- Dawei Du, Yuankai Qi, Hongyang Yu, Yifan Yang, Kaiwen Duan, Guorong Li, Weigang Zhang, Qingming Huang, and Qi Tian. The unmanned aerial vehicle benchmark: Object detection and tracking. In *Proceedings of the European conference on computer vision (ECCV)*, pages 370–386, 2018.
- Ruiyang Hao, Siqi Fan, Yingru Dai, Zhenlin Zhang, Chenxi Li, Yuntian Wang, Haibao Yu, Wenxian Yang, Jirui Yuan, and Zaiqing Nie. Rcooper: A real-world large-scale dataset for roadside cooperative perception. *arXiv preprint arXiv:2403.10145*, 2024.
- Yue Hu, Shaoheng Fang, Zixing Lei, Yiqi Zhong, and Siheng Chen. Where2comm: Communication-efficient collaborative perception via spatial confidence maps. *Advances in neural information processing systems*, 35:4874–4886, 2022.
- Jinlong Li, Runsheng Xu, Xinyu Liu, Baolu Li, Qin Zou, Jiaqi Ma, and Hongkai Yu. S2r-vit for multi-agent cooperative perception: Bridging the gap from simulation to reality. In *2024 IEEE International Conference on Robotics and Automation (ICRA)*, pages 16374–16380. IEEE, 2024a.
- Yiming Li, Shunli Ren, Pengxiang Wu, Siheng Chen, Chen Feng, and Wenjun Zhang. Learning distilled collaboration graph for multi-agent perception. *Advances in Neural Information Processing Systems*, 34:29541–29552, 2021.
- Yiming Li, Dekun Ma, Ziyang An, Zixun Wang, Yiqi Zhong, Siheng Chen, and Chen Feng. V2x-sim: Multi-agent collaborative perception dataset and benchmark for autonomous driving. *IEEE Robotics and Automation Letters*, 7(4):10914–10921, 2022.
- Zhenxin Li, Shiyi Lan, Jose M Alvarez, and Zuxuan Wu. Bevnex: Reviving dense bev frameworks for 3d object detection. In *Proceedings of the IEEE/CVF Conference on Computer Vision and Pattern Recognition*, pages 20113–20123, 2024b.
- Tsung-Yi Lin, Michael Maire, Serge Belongie, James Hays, Pietro Perona, Deva Ramanan, Piotr Dollár, and C Lawrence Zitnick. Microsoft coco: Common objects in context. In *Computer Vision—ECCV 2014: 13th European Conference, Zurich, Switzerland, September 6–12, 2014, Proceedings, Part V 13*, pages 740–755. Springer, 2014.
- Xuewu Lin, Tianwei Lin, Zixiang Pei, Lichao Huang, and Zhizhong Su. Sparse4d v2: Recurrent temporal fusion with sparse model. *arXiv preprint arXiv:2305.14018*, 2023.
- Haisong Liu, Yao Teng, Tao Lu, Haiguang Wang, and Limin Wang. Sparsebev: High-performance sparse 3d object detection from multi-camera videos. In *Proceedings of the IEEE/CVF International Conference on Computer Vision*, pages 18580–18590, 2023a.
- Yen-Cheng Liu, Junjiao Tian, Nathaniel Glaser, and Zsolt Kira. When2com: Multi-agent perception via communication graph grouping. In *Proceedings of the IEEE/CVF Conference on computer vision and pattern recognition*, pages 4106–4115, 2020a.
- Yen-Cheng Liu, Junjiao Tian, Chih-Yao Ma, Nathan Glaser, Chia-Wen Kuo, and Zsolt Kira. Who2com: Collaborative perception via learnable handshake communication. In *2020 IEEE International Conference on Robotics and Automation (ICRA)*, pages 6876–6883. IEEE, 2020b.

- Yingfei Liu, Tiancai Wang, Xiangyu Zhang, and Jian Sun. Petr: Position embedding transformation for multi-view 3d object detection. In *European Conference on Computer Vision*, pages 531–548. Springer, 2022.
- Yingfei Liu, Junjie Yan, Fan Jia, Shuailin Li, Aqi Gao, Tiancai Wang, and Xiangyu Zhang. Petr2: A unified framework for 3d perception from multi-camera images. In *Proceedings of the IEEE/CVF International Conference on Computer Vision*, pages 3262–3272, 2023b.
- Ze Liu, Yutong Lin, Yue Cao, Han Hu, Yixuan Wei, Zheng Zhang, Stephen Lin, and Baining Guo. Swin transformer: Hierarchical vision transformer using shifted windows. In *Proceedings of the IEEE/CVF international conference on computer vision*, pages 10012–10022, 2021.
- Zhijian Liu, Haotian Tang, Alexander Amini, Xinyu Yang, Huizi Mao, Daniela L Rus, and Song Han. Bevfusion: Multi-task multi-sensor fusion with unified bird’s-eye view representation. In *2023 IEEE international conference on robotics and automation (ICRA)*, pages 2774–2781. IEEE, 2023c.
- Cong Ma, Lei Qiao, Chengkai Zhu, Kai Liu, Zelong Kong, Qing Li, Xueqi Zhou, Yuheng Kan, and Wei Wu. Holovic: Large-scale dataset and benchmark for multi-sensor holographic intersection and vehicle-infrastructure cooperative. In *Proceedings of the IEEE/CVF Conference on Computer Vision and Pattern Recognition*, pages 22129–22138, 2024.
- Shital Shah, Debadeepta Dey, Chris Lovett, and Ashish Kapoor. Airsim: High-fidelity visual and physical simulation for autonomous vehicles. In *Field and Service Robotics: Results of the 11th International Conference*, pages 621–635. Springer, 2018.
- Pei Sun, Henrik Kretschmar, Xerxes Dotiwalla, Aurelien Chouard, Vijaysai Patnaik, Paul Tsui, James Guo, Yin Zhou, Yuning Chai, Benjamin Caine, et al. Scalability in perception for autonomous driving: Waymo open dataset. In *Proceedings of the IEEE/CVF conference on computer vision and pattern recognition*, pages 2446–2454, 2020.
- Shihao Wang, Yingfei Liu, Tiancai Wang, Ying Li, and Xiangyu Zhang. Exploring object-centric temporal modeling for efficient multi-view 3d object detection. In *Proceedings of the IEEE/CVF International Conference on Computer Vision*, pages 3621–3631, 2023.
- Tsun-Hsuan Wang, Sivabalan Manivasagam, Ming Liang, Bin Yang, Wenyuan Zeng, and Raquel Urtasun. V2vnet: Vehicle-to-vehicle communication for joint perception and prediction. In *Computer Vision—ECCV 2020: 16th European Conference, Glasgow, UK, August 23–28, 2020, Proceedings, Part II 16*, pages 605–621. Springer, 2020.
- Yue Wang, Vitor Campagnolo Guizilini, Tianyuan Zhang, Yilun Wang, Hang Zhao, and Justin Solomon. Detr3d: 3d object detection from multi-view images via 3d-to-2d queries. In *Conference on Robot Learning*, pages 180–191. PMLR, 2022.
- Hao Xiang, Zhaoliang Zheng, Xin Xia, Runsheng Xu, Letian Gao, Zewei Zhou, Xu Han, Xinkai Ji, Mingxi Li, Zonglin Meng, et al. V2x-real: a large-scale dataset for vehicle-to-everything cooperative perception. *arXiv preprint arXiv:2403.16034*, 2024.
- Runsheng Xu, Hao Xiang, Zhengzhong Tu, Xin Xia, Ming-Hsuan Yang, and Jiaqi Ma. V2x-vit: Vehicle-to-everything cooperative perception with vision transformer. In *European conference on computer vision*, pages 107–124. Springer, 2022a.
- Runsheng Xu, Hao Xiang, Xin Xia, Xu Han, Jinlong Li, and Jiaqi Ma. Opv2v: An open benchmark dataset and fusion pipeline for perception with vehicle-to-vehicle communication. In *2022 International Conference on Robotics and Automation (ICRA)*, pages 2583–2589. IEEE, 2022b.
- Runsheng Xu, Xin Xia, Jinlong Li, Hanzhao Li, Shuo Zhang, Zhengzhong Tu, Zonglin Meng, Hao Xiang, Xiaoyu Dong, Rui Song, et al. V2v4real: A real-world large-scale dataset for vehicle-to-vehicle cooperative perception. In *Proceedings of the IEEE/CVF Conference on Computer Vision and Pattern Recognition*, pages 13712–13722, 2023.

Haibao Yu, Yizhen Luo, Mao Shu, Yiyi Huo, Zebang Yang, Yifeng Shi, Zhenglong Guo, Hanyu Li, Xing Hu, Jirui Yuan, et al. Dair-v2x: A large-scale dataset for vehicle-infrastructure cooperative 3d object detection. In *Proceedings of the IEEE/CVF Conference on Computer Vision and Pattern Recognition*, pages 21361–21370, 2022.

Pengfei Zhu, Longyin Wen, Xiao Bian, Haibin Ling, and Qinghua Hu. Vision meets drones: A challenge. *arXiv preprint arXiv:1804.07437*, 2018.

Walter Zimmer, Gerhard Arya Wardana, Suren Sritharan, Xingcheng Zhou, Rui Song, and Alois C Knoll. Tumtraf v2x cooperative perception dataset. In *Proceedings of the IEEE/CVF Conference on Computer Vision and Pattern Recognition*, pages 22668–22677, 2024.

## A Appendix

### A.1 Annotation Statistics

We provide more details on the annotations of UAV3D here. There are 17 vehicle categories in UAV3D. As shown in Figure 5, the categories are almost evenly distributed as they were generated randomly from the simulation environment. In our benchmark experiments, we treated all vehicles as a single "car" class for the perception task. The 17 categories are available for more fine-grained perception tasks.

### A.2 UAV3D vs. CoPerception-UAVs

As shown in Table 11, UAV3D and CoPerception-UAVs are both UAV datasets that utilize simulations in Carla and AirSim, but they differ in several aspects. UAV3D includes more maps (Towns 3, 6, 7, and 10) compared to CoPerception-UAVs (Towns 3, 4, and 6) and operates with a static cross-shaped drone formation, while CoPerception-UAVs adopts a static V-shaped formation and a dynamic shape. Additionally, UAV3D provides 3D boxes, semantic labels, and box velocity as labels, whereas CoPerception-UAVs focus only on 3D boxes and semantic labels. UAV3D also significantly surpasses CoPerception-UAVs in terms of sample size, with 20,000 samples and 500,000 images, compared to 5,276 samples and 131,900 images in CoPerception-UAVs. Finally, UAV3D offers public access to its source code, while CoPerception-UAVs does not as of the release of the UAV3D benchmark.

Table 11: Comparison between CoPerception-UAVs and UAV3D.

	CoPerception-UAVs	UAV3D
Simulation	Carla & AirSim	Carla & AirSim
Maps	Town 3, 4 & 6	Town 3, 6, 7 & 10
Agents	5 drones	5 drones
Sensors	25 RGB cameras	25 RGB cameras
Height	40, 60, 80m	60m
Formation	Static V shape & Dynamic shape	Static cross-shape
#Categories	21	17
Frequency	0.25Hz	0.5Hz
Labels	3D boxes & Semantic labels	3D boxes & Semantic labels & Box velocity
#Samples	5,276	20,000
#Images	131,900	500,000
source code	×	✓

### A.3 Additional Experimental Results

For collaborative-UAV 3D object detection, we employ the additional metrics of Average Precision (AP) at Intersection-over-Union (IoU) thresholds of 0.5 and 0.7, following V2X-Sim Li et al. [2022]. Note that the orientation of boxes is not considered in our AP calculations. As shown in Table 12, the Upper-bound baseline has achieved the best performance and outperformed the Lower-bound baseline by a large gap of 0.213 in  $AP@0.5$  and 0.183 in  $AP@0.7$ . DiscoNet has achieved the best performance in the four collaborative baselines, with a slight performance gap of 0.087 in  $AP@0.5$  and 0.078 in  $AP@0.7$ , compared to the Upper-bound. The When2Com and Who2Com baselines have slightly better performance than the Lower-bound baseline since the fusion mechanism can only choose parts intermediate image features from other agents. The results of collaborative-UAV 3D object detection on test set are consistent with those observed on the validation set.

### A.4 UAV3D V1.0-mini

To facilitate the usage of UAV3D for perception tasks, a mini version of UAV3D (UAV3D V1.0-mini) has been created. UAV3D V1.0-mini is significantly smaller in size at just 7 GB, compared to the full UAV3D V1.0, which is approximately 400 GB. Despite the reduced size, UAV3D V1.0-mini includes 20 scenes captured from Town 10, with 400 samples and 10,000 images. In contrast, the full version, UAV3D V1.0, includes 1,000 scenes from multiple towns (Towns 3, 6, 7, and 10), providing 20,000 samples and 500,000 images. This mini version enables users to work with UAV3D more easily, particularly in environments with limited computational resources. The comparison between the UAV3D and UAV3D v1.0-mini is shown in Table 13.

Table 12: Collaborative-UAV 3D object detection results on the **validation** and **test** sets of UAV3D. The best results among all the methods are in bold.

Method	Validation set		Test set	
	AP@IoU=0.5 $\uparrow$	AP@IoU=0.7 $\uparrow$	AP@IoU=0.5 $\uparrow$	AP@IoU=0.7 $\uparrow$
Lower-bound	0.454	0.128	0.457	0.140
When2Com Liu et al. [2020a]	0.456	0.164	0.461	0.166
Who2Com Liu et al. [2020b]	0.447	0.161	0.453	0.141
V2VNet Wang et al. [2020]	0.537	0.169	0.545	0.141
DiscoNet Li et al. [2021]	0.580	0.233	0.649	0.247
Upper-bound	<b>0.667</b>	<b>0.311</b>	<b>0.673</b>	<b>0.316</b>

Table 13: Comparison between UAV3D V1.0-mini and UAV3D.

	UAV3D V1.0-mini	UAV3D
Maps	Town 10	Town 3, 6, 7&10
#scenes	20	1,000
#Samples	400	20,000
#Images	10,000	500,000
size	7GB	400 GB

Table 14: Single-UAV 3D object detection results on the validation set of UAV3D V1.0-mini.

Method	Dataset	Backbone	Size	mAP $\uparrow$	NDS $\uparrow$	mATE $\downarrow$	mASE $\downarrow$	mAOE $\downarrow$
PETR	V1.0-mini	Res-50	704 $\times$ 256	0.003	0.101	1.000	0.200	1.000
BEVFusion	V1.0-mini	Res-50	704 $\times$ 256	0.113	0.280	0.912	0.198	0.212
DETR3D	V1.0-mini	Res-50	704 $\times$ 256	0.023	0.114	1.000	0.197	1.000
PETR	V1.0-mini	Res-50	800 $\times$ 450	0.005	0.103	1.000	0.198	1.000
BEVFusion	V1.0-mini	Res-101	800 $\times$ 450	0.112	0.273	0.947	0.195	0.232
DETR3D	V1.0-mini	Res-101	800 $\times$ 450	0.051	0.174	1.000	0.195	0.663

Table 15: Collaborative-UAV 3D object detection results on the validation set of UAV3D V1.0-mini.

Method	Dataset	mAP $\uparrow$	NDS $\uparrow$	mATE $\downarrow$	mASE $\downarrow$	mAOE $\downarrow$
Lower-bound	V1.0-mini	0.147	0.304	0.933	0.192	0.176
When2Com	V1.0-mini	0.151	0.310	0.922	0.193	0.156
Who2Com	V1.0-mini	0.153	0.314	0.899	0.193	0.161
V2VNet	V1.0-mini	0.265	0.390	0.855	0.192	0.152
DiscoNet	V1.0-mini	0.218	0.322	0.886	0.193	0.431
Upper-bound	V1.0-mini	0.349	0.468	0.656	0.190	0.153

**Experimental Results** Table 14 reports the results of single-UAV 3D object detection on the validation set of UAV3D V1.0-mini. Among these models, BEVFusion consistently achieves the best performance across all five metrics, including mAP, NDS, mATE, mASE, and mAOE. PETR, on the other hand, shows the worst overall performance and is particularly sensitive to the scale of the training dataset. When larger backbone models (ResNet-101) and larger input image sizes (800 $\times$ 450) are used, DETR3D demonstrates modest improvement in its detection performance, while PETR and BEVFusion show almost no improvement.

Table 15 shows the collaborative-UAV 3D object detection results on the validation set of UAV3D V1.0-mini. Among the four collaborative baselines, V2VNet achieves the best performance with mAP of 0.265 and NDS of 0.390, outperforming When2Com, Who2Com, and DiscoNet. DiscoNet performs relatively well, showing higher performance in mAP and NDS compared to When2Com and Who2Com, though it suffers from a high mAOE of 0.431. The lower-bound baseline has the worst performance, while the upper-bound baseline provides the best performance with mAP of 0.349 and NDS of 0.468.

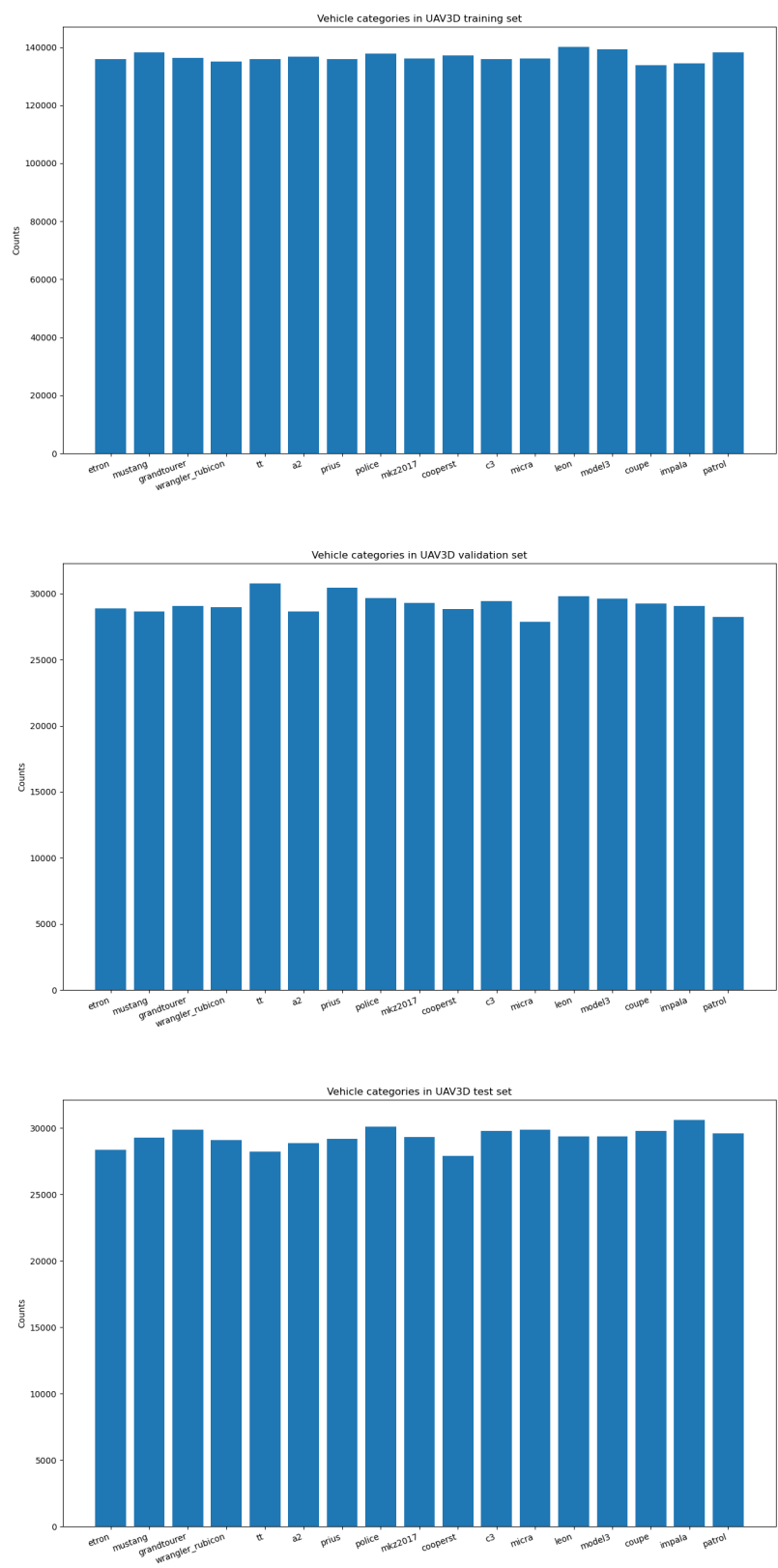


Figure 5: Number of annotations per category in UAV3D training, validation and test set. The vehicle categories are almost evenly distributed.



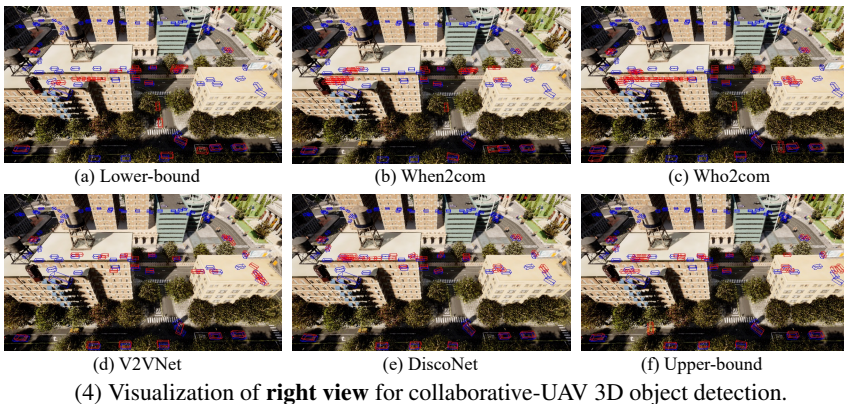
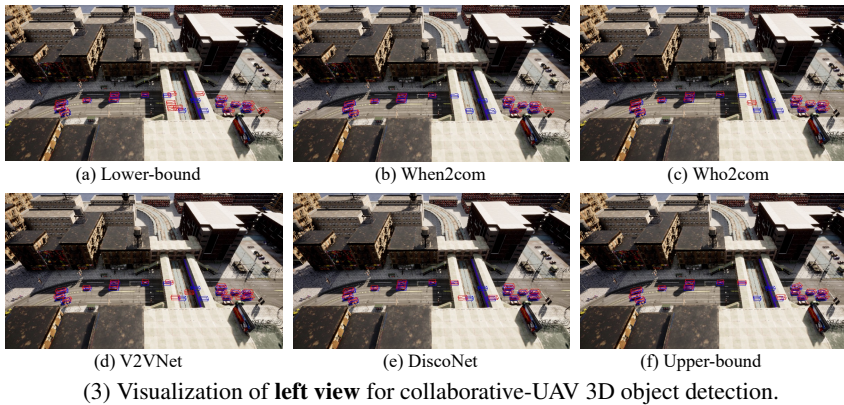
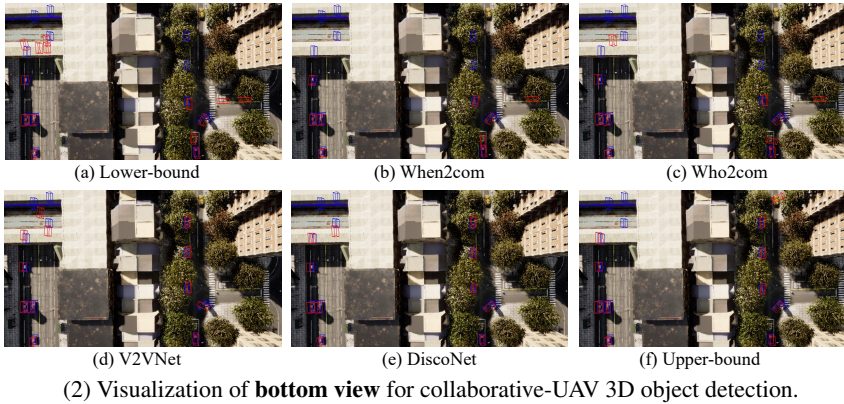
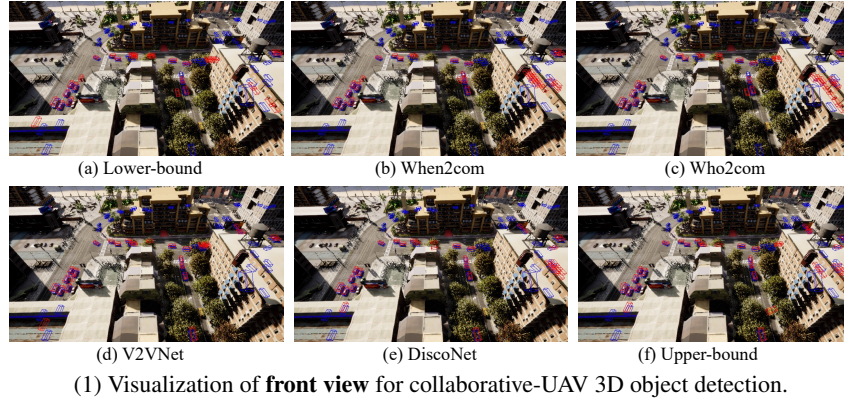


Figure 6: Visualizations of collaborative-UAV 3D object detection results on UAV3D. Red boxes represent the predictions, while blue boxes indicate the ground truth.